DPCM FOR QUANTIZED BLOCK-BASED COMPRESSED SENSING OF IMAGES

Sungkwang Mun and James E. Fowler
Department of Electrical and Computer Engineering, Geosystems Research Institute,
Mississippi State University, USA

ABSTRACT

Differential pulse-code modulation is coupled with uniform scalar quantization to provide block-based quantized compressed sensing of images. Experimental results demonstrate significant improvement in rate-distortion performance as compared scalar quantization used alone in several block-based compressed-sensing reconstruction algorithms. Additionally, rate-distortion performance superior to that of alternative quantized-compressed-sensing techniques relying on optimized quantization or reconstruction is observed.

Index Terms— Compressed sensing, quantization, DPCM

1. INTRODUCTION

Recent literature has seen an explosion of interest in compressed sensing (CS). Much attention has been devoted to the CS of still images, with both sensing architectures (e.g., [1]) and image-reconstruction algorithms (e.g., [2–7]) being proposed. In most CS literature, the CS measurement process—typically a linear projection into a lower-dimensional subspace chosen at random—is assumed to take place within the hardware of the sensing device. Consequently, the CS measurement process can thus be considered to effectuate signal acquisition and dimensionality reduction simultaneously. However, in and of itself, this dimensionality reduction obtained by the CS measurement process does not produce compression in the strict information-theoretic sense; indeed, some form of quantization is necessary to produce a compressed bitstream from the CS measurements. Although such quantization is unavoidable in any real-life implementation of a CS measurement scheme, CS literature has largely avoided the topic of quantization.

The straightforward solution to incorporating quantization into the CS paradigm is simply to apply scalar quantization (SQ) to each of the CS measurements produced by the sensing device. However, it has been established that such an SQ-based solution is highly inefficient in terms of information-theoretic rate-distortion performance as compared to traditional source-coding techniques (e.g., [8]). As a consequence, there have been a variety of efforts in recent literature aimed at the improvement of rate-distortion performance of quantized CS, largely through an optimization of the quantization process (e.g., [9]), the reconstruction process (e.g., [10, 11]), or both (e.g., [12, 13]).

In contrast to prior work on quantized CS which largely relies on optimized quantization or reconstruction, we propose a straightforward process of quantization via simple uniform SQ applied in conjunction with differential pulse code modulation (DPCM) of the CS measurements. Our framework is applicable only to the CS of images effectuated in blocks, i.e., block-based CS (BCS) [2–6]. In essence, at the sensor side of the system, rather than applying quantization directly to each block of CS measurements, a prediction of the block is made and subtracted from the current block of measurements in the measurement domain. The resulting residual is then scalar-quantized. At the reconstruction side of the system, the same prediction is added onto the dequantized residuals to produce the quantized CS measurements ready for BCS-based reconstruction.

A key benefit of our proposed DPCM-based methodology is that both the BCS-based sensor as well as the BCS-based reconstruction are unmodified; in fact, the latter can be any BCS-based reconstruction. While the sensor device does incur some additional complexity, the addition of the DPCM processing (a subtraction) is not substantially more burdensome than the already-necessary SQ. Experimental results using state-of-the-art BCS-based reconstruction algorithms on still images demonstrate that, not only does this simple DPCM-plus-SQ approach to quantized CS provide rate-distortion performance surprisingly competitive with that of alternative approaches such as [11, 13], it can occasionally rival traditional image coding in the form of JPEG, particularly at low bitrates.

2. BACKGROUND

In brief, CS is a mathematical paradigm which permits, under certain conditions, signals to be acquired via linear projection into a dimension much lower than that of the original signal, yet which still allows exact recovery of the signal from the measurements. More specifically, suppose that we want to recover real-valued signal $\mathbf{x}$ with length N from M measurements such that $M \ll N$. In other words, we want to recover $\mathbf{x}$ from $\mathbf{y} = \mathbf{\Phi x}$, where $\mathbf{y}$ has length M, and $\mathbf{\Phi}$ is an $M \times N$ measurement matrix with subsampling rate, or *subrate*, being $S = M/N$. Because the number of

This material is based upon work supported by the National Science Foundation under Grant No. CCF-0915307.

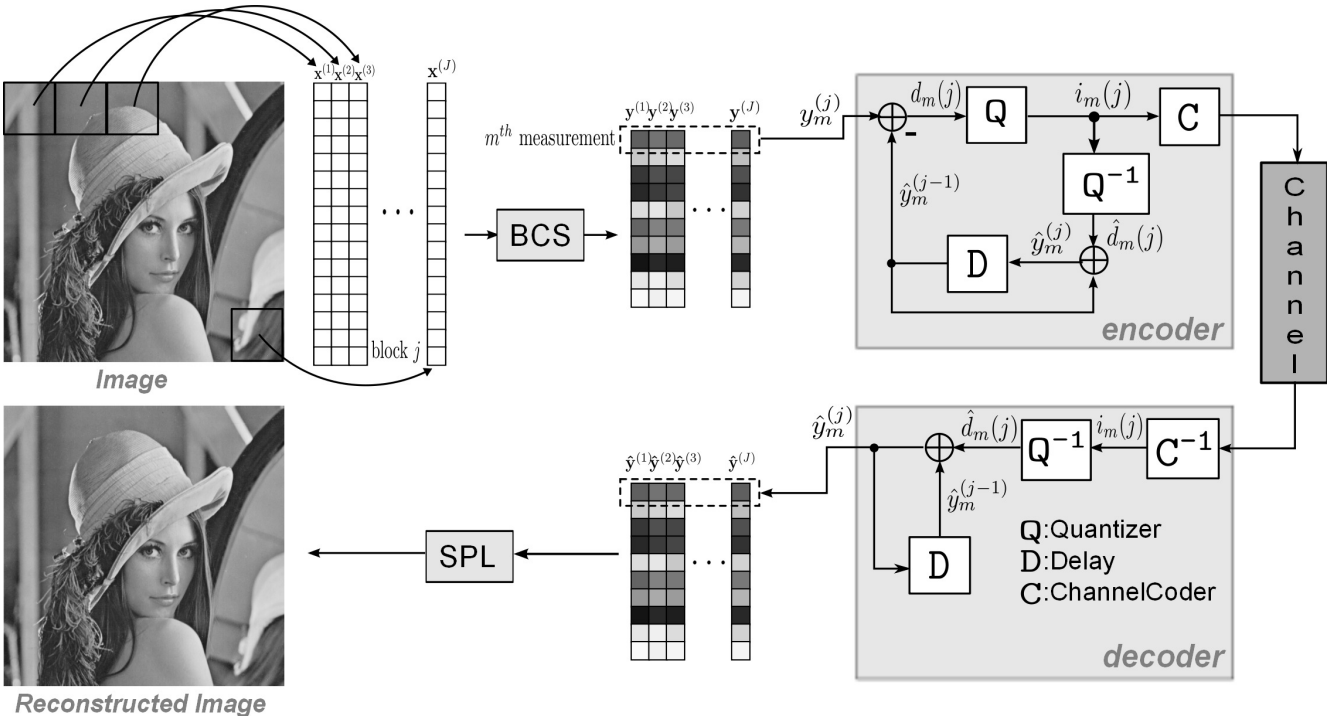

Figure 1: Application of DPCM and SQ to the BCS-SPL architecture of [3]. BCS is implemented with any CS-based image-acquisition, such as the single-pixel camera of [1]; Q is uniform SQ; D is a single-block delay buffer; and C is any entropy coder, such as arithmetic coding.

unknowns is much larger than the number of observations, recovering every $\mathbf{x} \in \Re^N$ from its corresponding $\mathbf{y} \in \Re^M$ is impossible in general; however, if $\mathbf{x}$ is sufficiently sparse in some domain, then exact recovery of $\mathbf{x}$ is possible—this is the fundamental tenet of CS theory.

In BCS, an image is divided into $B \times B$ blocks and sampled using an appropriately-sized measurement matrix. That is, suppose that $\mathbf{x}^{(j)}$ is a vector representing, in raster-scan fashion, block j of input image $\mathbf{x}$. The corresponding $\mathbf{y}^{(j)}$ is then $\mathbf{y}^{(j)} = \mathbf{\Phi}_B \mathbf{x}^{(j)}$, where $\mathbf{\Phi}_B$ is an $M_B \times B^2$ measurement matrix such that the subrate for the image as a whole is $S = M_B/B^2$. It is straightforward to see that $\mathbf{\Phi}_B$ applied block-by-block to an image is equivalent to a whole-image measurement matrix $\mathbf{\Phi}$ with a constrained structure; specifically, $\mathbf{\Phi}$ is constrained to be block diagonal with $\mathbf{\Phi}_B$ along the diagonal.

In [2], BCS was proposed wherein the sampling of an image is driven by random matrices applied on a block-by-block basis, while the reconstruction is a variant of projected Landweber (PL) reconstruction that incorporates a smoothing operation intended to reduce blocking artifacts. Since it combines BCS with a smoothed PL (SPL) reconstruction, in [3], the overall technique was called BCS-SPL. BCS-SPL was extended to incorporate block-based measurement in the domain of a wavelet transform in [4]; the resulting multiscale approach was called MS-BCS-SPL. A further extension of BCS-SPL was presented in [5] wherein multiple predictions were culled from the image being reconstructed, following which reconstruction was driven by the measurement-domain residual resulting from the predictions. This latter technique was called multihypothesis BCS-SPL (MH-BCS-SPL) in [5].

3. DPCM FOR QUANTIZED BCS

Effectively, our proposed approach applies DPCM and SQ onto the CS measurements within the BCS-SPL architecture of [3] as shown in Fig. 1. On the sensor side of the system, BCS measurements are acquired as usual using $B \times B$ blocks from the original image, producing M-dimensional measurement vector

$$\mathbf{y}^{(j)} = \begin{bmatrix} y_1^{(j)} & \cdots & y_m^{(j)} & \cdots & y_{M_B}^{(j)} \end{bmatrix}^T = \mathbf{\Phi}_B \mathbf{x}^{(j)} \quad (1)$$

for block j of the image, $\mathbf{x}^{(j)}$. For component m in measurement vector $\mathbf{y}^{(j)}$, a prediction is subtracted and the residual is scalar-quantized. Specifically, to predict $y_m^{(j)}$, we use the corresponding vector component of the previously processed block $\hat{\mathbf{y}}^{(j-1)}$. That is, the residual $d_m^{(j)} = y_m^{(j)} - \hat{y}_m^{(j-1)}$ is scalar-quantized to produce quantization index $i_m^{(j)} = Q\left[d_m^{(j)}\right]$ which is then entropy coded. The DPCM

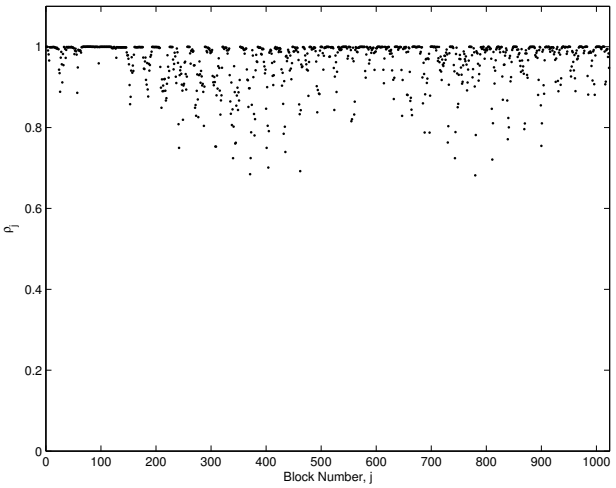

Figure 2: Correlation coefficient ρ_j between current block $\mathbf{y}^{(j)}$ and preceding block $\mathbf{y}^{(j-1)}$ for the 512×512 Lenna image. Blocks of size 16×16 are extracted from the image and subject to random projection with a subrate of 0.5. Average correlation over all blocks is $\bar{\rho} = 0.971$.

feedback loop consists of dequantization of $i_m^{(j)}$, producing the quantized residual, $\hat{d}_m^{(j)} = Q^{-1}\left[i_m^{(j)}\right]$ such that $\hat{y}_m^{(j)} = \hat{d}_m^{(j)} + \hat{y}_m^{(j-1)}$. Finally, the prediction is implemented with a one-block delay buffer. We note that the set of measurements in the first block is processed in the same manner by initializing $\hat{\mathbf{y}}^{(0)}$ to be the zero vector.

In general, DPCM works when signals possess a significant degree of correlation from one time to the next. Such correlation typically exists in images from one image block to the next, and random projection in the form of $\mathbf{y}^{(j)} = \mathbf{\Phi}_B \mathbf{x}^{(j)}$ preserves this correlation. For example, we define the measurement-domain correlation coefficient between blocks $\mathbf{y}^{(j)}$ and $\mathbf{y}^{(j-1)}$ as

$$\rho_j = \frac{{\mathbf{y}^{(j)}}^T \mathbf{y}^{(j-1)}}{\left\|\mathbf{y}^{(j)}\right\| \left\|\mathbf{y}^{(j-1)}\right\|}. \qquad (2)$$

Fig. 2 plots ρ_j for a single grayscale image; we see that, for many blocks, ρ_j is close to 1.0, while the average correlation over all blocks, $\bar{\rho} = 0.971$, indicates that the consecutive blocks are typically highly correlated, even in the measurement domain.

The basic approach of Fig. 1, which illustrates our proposed framework for the incorporation of DPCM into BCS-SPL, can also be applied to the MS-BCS-SPL [4] and MH-BCS-SPL [5] variants. Specifically, for the former, wavelet-domain blocks in the baseband are fed into the DPCM encoder, while the other subbands are quantized directly with uniform SQ (unlike the baseband coefficients, those in the other subbands have low correlation). For the latter, the DPCM encoder processes the same measurements as those of the original BCS-SPL without reserving a holdset for cross-validation.

We mention that our proposed DPCM-based approach bears some resemblance to the sigma-delta quantization for CS in [14] in the sense that sigma-delta modulation also provides quantization based on differences between CS measurements. Our approach is somewhat simpler conceptually ([14] requires Sobolev frames for reconstruction); additionally, we apply DPCM across blocks rather than sample-by-sample as in the sigma-delta modulation of [14].

4. RESULTS

We now present experimental results that demonstrate the performance of the proposed technique for DPCM-based quantized CS. We first examine the rate-distortion efficiency of DPCM plus SQ by comparing it to simple uniform SQ applied alone to the BCS measurements. We use several BCS-based algorithms—namely, the original BCS-SPL from [3] as well as the MS-BCS-SPL and MH-BCS-SPL extensions from [4] and [5], respectively—and deploy DPCM plus SQ in the framework presented in Fig. 1 to effectuate quantized CS for all three methods. We note that the implementations of BCS-SPL, MS-BCS-SPL, and MH-BCS-SPL can be found at the BCS-SPL website[1].

All experiments use 512×512 grayscale images, and we measure rate-distortion performance in terms of peak signal-to-noise ratio (PSNR) in dB and bitrate in bits per pixel (bpp) using the entropy of the quantizer indices as an estimate of the actual bitrate that would be produced by a real entropy coder. The measurement matrix $\mathbf{\Phi}_B$ is an orthonormalized dense Gaussian random matrix, and a 5-level dual-tree discrete wavelet transform (DDWT) [15] is used as the sparsity basis for all three methods. A BCS block size of $B = 16$ was used for both BCS-SPL and MH-BCS-SPL, while MS-BCS-SPL uses $B = 2$ for each of the levels within the wavelet-based measurement basis. All SQ is uniform. Finally, we note that, for both SQ as well as DPCM plus SQ, the bitrate obtained depends on both the stepsize of the scalar quantizer as well as the subrate $S = M_B/B^2$ of the BCS measurement process. In all cases, for the experiments here, the optimal combination of quantizer stepsize and subrate is chosen via an exhaustive search over all possible (stepsize, subrate) pairs drawn from a finite set of stepsizes and a finite set of subrates.

Table 1 compares the PSNR performance at a fixed bitrate of 0.5 bpp for the three BCS-based techniques, BCS-SPL, MS-BCS-SPL, and MH-BCS-SPL. We see that, for all three algorithms, the addition of DPCM to the quantization process increases the PSNR by 0.5 to 1.0 dB on average as compared to simply using SQ alone.

Figs. 3–6 present the rate-distortion performance for all

[1] `http://www.ece.msstate.edu/~fowler/BCSSPL/`

three BCS-based techniques using the proposed DPCM plus SQ framework for a bitrate ranging from 0.1 to 1.0 bpp. Additionally, Figs. 3–6 include as benchmarks two other quantized-CS approaches—MARX [7] reconstruction using the progressive quantization (PQ) proposed in [12], and basis pursuit dequantizer (BPDQ)[2] [11]. Finally, we also include the rate-distortion performance of JPEG as indicative of the performance of a relatively simple image coder built with traditional source-coding techniques. Generally, we see that the DPCM-based MS-BCS-SPL reconstruction outperforms the other quantized-CS techniques; however, traditional source-coding in the form of JPEG achieves the best rate-distortion performance, except at low bitrates (0.2 bpp and below) where MS-BCS-SPL with DPCM yields higher PSNR.

5. CONCLUSION

In this paper, we proposed the incorporation of DPCM to achieve quantized CS of images based on blocks. In essence, we used one measurement-domain block to predict the next, applying uniform SQ to the measurement-domain residual of the prediction. Experimental results demonstrated an improvement of 0.5 to 1 dB in rate-distortion performance as compared to BCS-based image reconstruction using uniform SQ alone. Additionally, rate-distortion performance superior to alternative quantized-CS schemes relying on optimized quantization or reconstruction was observed.

6. ACKNOWLEDGMENT

The authors thank L. Wang and X. Wu for providing source code for their implementations of algorithms in [12, 13].

7. REFERENCES

[1] M. F. Duarte, M. A. Davenport, D. Takhar, J. N. Laska, T. Sun, K. F. Kelly, and R. G. Baraniuk, "Single-pixel imaging via compressive sampling," *IEEE Signal Processing Magazine*, vol. 25, no. 2, pp. 83–91, March 2008.

[2] L. Gan, "Block compressed sensing of natural images," in *Proceedings of the International Conference on Digital Signal Processing*, Cardiff, UK, July 2007, pp. 403–406.

[3] S. Mun and J. E. Fowler, "Block compressed sensing of images using directional transforms," in *Proceedings of the International Conference on Image Processing*, Cairo, Egypt, November 2009, pp. 3021–3024.

[4] J. E. Fowler, S. Mun, and E. W. Tramel, "Multiscale block compressed sensing with smoother projected Landweber reconstruction," in *Proceedings of the European Signal Processing Conference*, Barcelona, Spain, August 2011, pp. 564–568.

[5] C. Chen, E. W. Tramel, and J. E. Fowler, "Compressed-sensing recovery of images and video using multihypothesis predictions," in *Proceedings of the 45th Asilomar Conference on Signals, Systems, and Computers*, Pacific Grove, CA, November 2011, pp. 1193–1198.

[6] J. E. Fowler, S. Mun, and E. W. Tramel, "Block-based compressed sensing of images and video," *Foundations and Trends in Signal Processing*, vol. 4, no. 4, pp. 297–416, March 2012.

[7] X. Wu, X. Zhang, and J. Wang, "Model-guided adaptive recovery of compressive sensing," in *Proceedings of the Data Compression Conference*, J. A. Storer and M. W. Marcellin, Eds., Snowbird, UT, March 2009, pp. 123–132.

[8] V. K. Goyal, A. K. Fletcher, and S. Rangan, "Compressive sampling and lossy compression," *IEEE Signal Processing Magazine*, vol. 25, no. 2, pp. 48–56, March 2008.

[9] J. Z. Sun and V. K. Goyal, "Optimal quantization of random measurements in compressed sensing," in *Proceedings of the IEEE International Symposium on Information Theory*, Seoul, Korea, June 2009, pp. 6–10.

[10] P. T. Boufounos and R. G. Baraniuk, "1-bit compressive sensing," in *Proceedings of the 42nd Annual Conference on Information Sciences and Systems*, Princeton, NJ, March 2008, pp. 16–21.

[11] L. Jacques, D. K. Hammond, and J. M. Fadili, "Dequantizing compressed sensing: When oversampling and non-Gaussian constraints combine," *IEEE Transactions on Information Theory*, vol. 57, no. 1, pp. 559–571, January 2011.

[12] L. Wang, X. Wu, and G. Shi, "Progressive quantization of compressive sensing measurements," in *Proceedings of the Data Compression Conference*, J. A. Storer and M. W. Marcellin, Eds., Snowbird, UT, March 2011, pp. 233–242.

[13] ——, "Binned progressive quantization for compressive sensing," *IEEE Transactions on Image Processing*, vol. 21, no. 6, pp. 2980–2990, June 2012.

[14] C. S. Güntürk, M. Lammers, A. Powell, R. Saab, and Ö. Yılmaz, "Sobolev duals for random frames and sigma-delta quantization of compressed sensing measurements," submitted.

[15] N. G. Kingsbury, "Complex wavelets for shift invariant analysis and filtering of signals," *Journal of Applied Computational Harmonic Analysis*, vol. 10, pp. 234–253, May 2001.

[2] `http://wiki.epfl.ch/bpdq`

Table 1: PSNR Performance in dB for a bitrate of 0.5 bpp

	BCS-SPL			MS-BCS-SPL			MH-BCS-SPL		
Image	SQ	DPCM	*Gain*	SQ	DPCM	*Gain*	SQ	DPCM	*Gain*
Lenna	27.7	29.4	+1.7	33.9	34.7	+0.9	29.2	30.7	+1.5
Barbara	22.9	23.6	+0.7	26.6	27.4	+0.8	27.3	28.2	+0.9
Peppers	28.6	29.5	+0.9	33.8	34	+0.2	29.6	30.3	+0.7
Goldhill	26.7	27.4	+0.7	30.6	31	+0.5	27.0	28.2	+1.2
Man	26.2	26.9	+0.7	30.5	30.7	+0.2	26.5	27.3	+0.8
Clown	26.7	27.6	+0.9	32.7	33.2	+0.5	28.8	29.8	+1.0
Average	26.5	27.4	+0.9	31.3	31.8	+0.5	28.1	29.1	+1.0

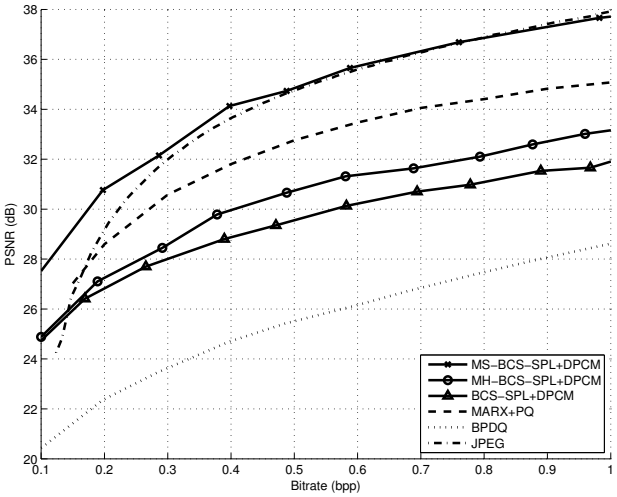

Figure 3: Rate-distortion performance for Lenna

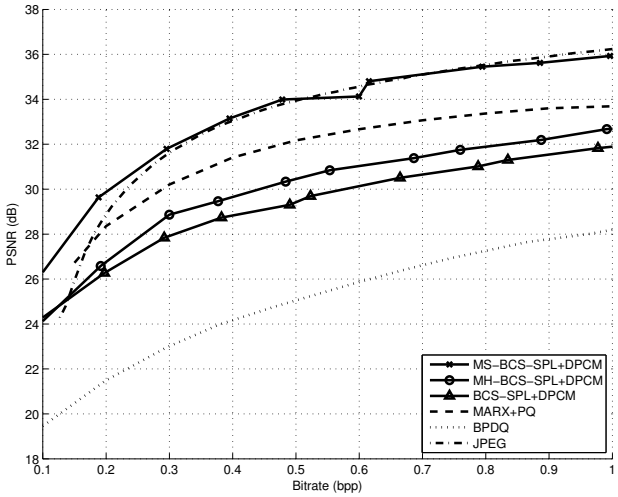

Figure 5: Rate-distortion performance for Peppers

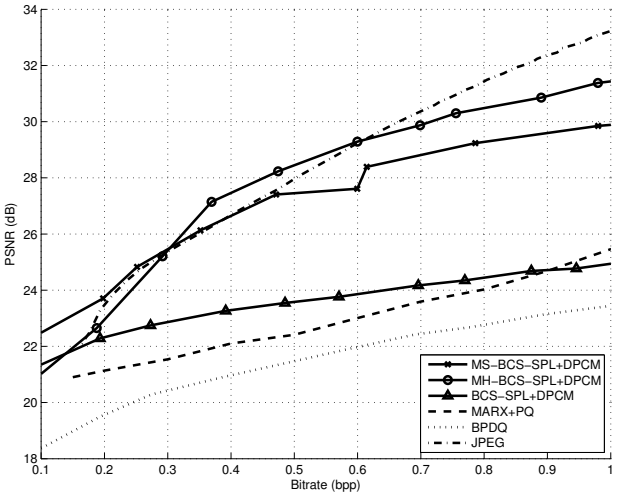

Figure 4: Rate-distortion performance for Barbara

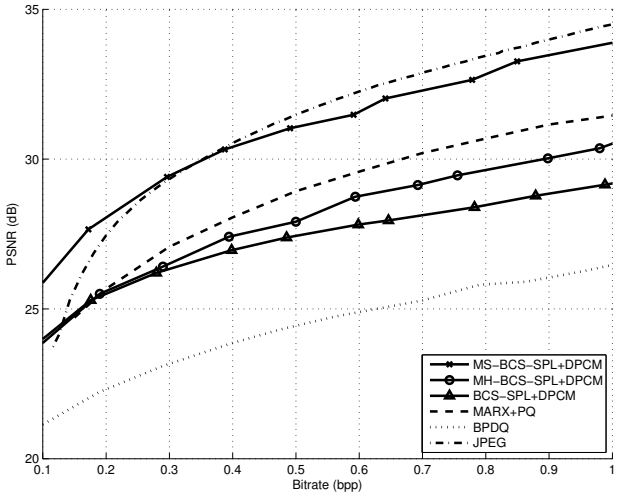

Figure 6: Rate-distortion performance for Goldhill